Incorporation of Rhodopsin in Laterally Structured Supported Membranes: Observation of Transducin Activation with Spatially and Time-Resolved Surface Plasmon Resonance†

Stephan Heyse,‡ Oliver P. Ernst,§ Zoltan Dienes,‡,|| Klaus Peter Hofmann,§ and Horst Vogel*,‡

Laboratory of Physical Chemistry of Polymers and Membranes, Chemistry Department, Swiss Federal Institute of Technology, CH-1015 Lausanne, Switzerland, and Institut für Medizinische Physik und Biophysik, Universitätsklinikum Charité, Humboldt-Universität, D-10098 Berlin, Germany

Received June 30, 1997; Revised Manuscript Received October 21, 1997

ABSTRACT: Rhodopsin−transducin coupling was used as an assay to investigate a laterally patterned membrane reconstituted with a receptor and its G protein. It served as a model system to show the feasibility to immobilize G protein-coupled receptors on solid supports and investigate receptor activation and interaction with G proteins by one-dimensional imaging surface plasmon resonance. Supported membranes were formed by the self-assembly of lipids and rhodopsin from detergent solution onto functionalized gold surfaces. They formed micrometer-sized alternating regions of pure fluid phospholipid bilayers separated by bilayers composed of an outer phospholipid leaflet on a gold-attached inner thiolipid. Rhodopsin was found to incorporate preferentially into the phospholipid bilayer regions, whereas transducin was uniformly distributed over the entire outer surface of the supported patterned membrane. The influence of rhodopsin on the dark binding of transducin to lipid membranes was described quantitatively and compared with previously published data. Coupling reactions with transducin resembled closely the native system, indicating that the native functionality of rhodopsin was preserved in the supported membranes. The spatially varying properties of the membranes resulted in a pattern of rhodopsin activity on the surface. This combination of techniques is very promising for the investigation of the lateral diffusion of transducin, can be extended to include signalling proteins downstream of the G protein, and may be applied to functional screening of other G protein-coupled receptors. In the future, it may also serve as a basis for constructing biosensors based on receptor proteins.

Many central biological signal recognition and transduction processes such as G protein-coupled receptor (GPCR)[1] amplification cascades occur at the level of cell membranes (*1*). The biological function of the respective membrane receptors is modulated by soluble active substances. Both the functional understanding of molecular recognition processes leading to activation of receptors as well as their use in screening for effector compounds are important aspects in basic research and drug discovery. With the increasing number of membrane receptor targets and the emergence of combinatorial libraries of compounds, there is a strong need to develop novel, highly sensitive, and fast assays for ligand−receptor interaction and receptor function. At present, screening for new pharmacologically active compounds still follows traditional routes applying time-consuming ligand binding studies (e.g., by using radioactively labeled compounds) and separate receptor function tests (*2*).

An important family of receptors are the GPCRs, integral membrane proteins that transmit signals into cells in response to a variety of extracellular stimuli such as hormones, ions, or even light. They are believed to have seven transmembrane helices and to interchange between a number of different conformations that can selectively bind ligands and activate G proteins with important functional consequences (*3, 4*).

It is the topic of the present work to develop new functional tests with GPCR which are generally applicable for membrane-bound receptors. As a first step toward this goal, we realize a functional assay for the photoreceptor rhodopsin with its G protein transducin. The methodology

† This work was supported financially by the Swiss National Science Foundation Priority Programme on Biotechnology, Grant 5002-35180 (H.V.), and by the Deutsche Forschungsgemeinschaft, SFB 366, and the Fonds der Chemischen Industrie (K.P.H.).

* Corresponding author. Fax: ++41 21 693 6190. Phone: ++41 21 693 6188. E-mail: Horst.Vogel@icp.dc.epfl.ch.

‡ Swiss Federal Institute of Technology.

§ Humboldt-Universität.

|| Present address: Firmenich SA, CH-1283 La Plaine, Geneva, Switzerland.

[1] Abbreviations: 2D, two-dimensional; BTP, Bis-Tris Propane (1,3-bis[tris(hydroxymethyl)methylamino]propane); CCD, charge coupled device; CMC, critical micelle concentration; CTA, 11-mercaptoundecanoic acid; DCC, *N*,*N*′-dicyclohexylcarbodiimide; DIEA, *N*,*N*-diisopropylethylamine; EDTA, ethylenediaminetetraacetic acid; egg-PC, egg phosphatidylcholine; EM, electron microscopy; G_t, transducin; GDP, guanosine 5′-diphosphate; GPCR, G protein-coupled receptor; GTP, guanosine 5′-triphosphate; MI/MII/MIII, rhodopsin in the meta I/meta II/meta III states; NHS, *N*-hydroxysuccinimide; OG, octyl β-D-glucoside; POPC, 1-palmitoyl-2-oleoyl-3-*sn*-phosphatidylcholine; POPE, 1-palmitoyl-2-oleoyl-3-*sn*-phosphatidylethanolamine; R*, photoexcited rhodopsin; ROS, rod outer segments; SPR, surface plasmon resonance; 1D-SPR, one-dimensional imaging SPR; TEA, triethylamine; TFA, trifluoroacetic acid; TOF-SIMS, time-of-flight secondary ion mass spectrometry; UV, ultraviolet light.

S0006-2960(97)01564-X CCC: $15.00
Published on Web 01/13/1998

applied will be transferable to ligand-activated G protein-coupled receptors. In the following, we present the general strategy and concept of our development.

The Receptor System. We have chosen rhodopsin as an example of a GPCR, first because the visual signal cascade is biochemically and biophysically well-characterized [for reviews, see, e.g., (*3, 5*−*7*)], and second, because rhodopsin and other components of the cascade are available in high purity and in chemical amounts (*8*). Although triggered by light, the visual cascade shares many properties with the signal cascades of ligand-activated GPCRs, for example, the mechanism of receptor conformational changes following the trigger, the role of the cytoplasmic surface of receptors in G protein coupling, and receptor shut-off mechanisms [reviewed in (*7*)]. Rhodopsin itself has been studied using a variety of biophysical techniques, giving information on its structure in the membrane (*9*), on its rotational and translational diffusion (*10*−*12*), and on the influence of lipid environment on its function (*13*−*15*). The activation of rhodopsin by light offers a unique opportunity to resolve fast reactions in the signal amplification cascade without the need to consider ligand accessibility and orientational effects (*16*−*19*). Knowledge of the major partial reactions and the relative simplicity and linearity of the signal pathway make an interpretation possible in terms of quantitative models (*20*−*22*).

Detection of the Interaction of G Protein with Its Activated Receptor. Any functional assay for GPCRs must rely on detection of the signalling state(s) of the receptor itself [for example, by FTIR (*23*) or by measurement of proton uptake (*24*)], or at least one of the signal transmitter reactions following the activation of the receptor. Two different strategies exist for such a functional assay: Either the GPCR is expressed in suitable cells and used in this form for the investigations (*25*), or it is isolated in natural membrane fragments, and if necessary purified and reconstituted into artificial lipid bilayers (*7, 19, 26, 27*).

Surface-sensitive optical techniques based on evanescent waves (*28, 29*) are ideally suited for the second strategy. Here the receptor and/or the corresponding interacting molecules (e.g., G proteins) are immobilized on a suitable sensor surface, and the binding of the complementary partner is detected. Thanks to the surface immobilization of one of the interacting partners, these methods can directly distinguish between free and receptor-bound ligands without additional separation steps. Such techniques may be more generally applicable than the biophysical methods already available for special cases [such as kinetic light scattering or stabilization assays, see, e.g., (*30*) in case of rhodopsin].

In the present work, we concentrate on surface plasmon resonance (SPR) as the detection technique because it offers several important advantages for investigating interactions at membrane surfaces: (i) It measures directly the amount of bound analyte molecules at the sensor surface without additional labeling of the interacting molecules. (ii) The chemical immobilization procedures are well developed (covalent attachment of sulfur-bearing molecules to gold surfaces) (*31, 32*). (iii) All steps of the immobilization and reconstitution procedure can be observed individually.

Reconstitution of GPCR into Supported Lipid Membranes. In order to dissect the complicated signal amplification cascade of GPCR into individually controllable steps, the rhodopsin/G protein couple was reconstituted in artificial lipid bilayers supported on the sensor surface. For water-soluble receptors, immobilization procedures on sensor surfaces are well-developed (*33, 34*, and references therein), in contrast to only a few examples for membrane proteins, requiring supported membranes (*35, 36*).

General constraints on the functional reconstitution of a transmembrane protein are a fluid membrane environment and aqueous phases on both sides of the membrane which are sufficiently large to accommodate the extramembranous parts of the protein. On hydrophilic supports (e.g., SiO_2), fluid lipid bilayers can be formed by spontaneous fusion of lipid vesicles to the surfaces (*37, 38*), although the success of this process critically depends on the properties of both the supporting surface and the lipid vesicles and is not yet fully understood (*39*). The bilayers "float" on a water film a few tens of angstroms thick (*40*). To link the membranes more stably to the support while preserving the advantages of "floating" membranes, novel concepts have been developed recently to control the formation of supported lipid bilayers and to mechanically stabilize them by anchoring them to the surface via hydrophilic spacers (*32, 41*).

We have addressed this issue by synthesizing a new class of lipid molecules, the thiolipids, which were created to form stable supported lipid bilayers on gold. A typical thiolipid molecule consists of a glycerophospholipid moiety attached via its polar headgroup to a hydrophilic spacer of variable length.

Micropatterned Arrays of Fluid Lipid Bilayers. Here we use these anchored lipid membranes in a novel way to create micropatterned arrays of fluid lipid bilayers. We show that these bilayers are suitable for the functional reconstitution of the membrane protein rhodopsin. The concept is depicted in Figure 1. The lipid membrane on the gold surface of the SPR transducer consists of micrometer-sized regions of fluid phospholipid bilayers separated by fluid phospholipid monolayers (assembled on a rigid, gold-attached thiolipid monolayer). The fluid lipid bilayers should serve as a suitable matrix for reconstituting the transmembrane receptor protein in a functionally active form, whereas the fluid lipid monolayer regions should hinder the insertion of receptors. In contrast, the G proteins simply partition to the membrane−water interface and should therefore be distributed uniformly over the entire outer surface of the supported lipid mono- and bilayers.

In the case of functionally correct reconstitution, after receptor activation, the G protein transducin will interact with rhodopsin, dissociate, and release the active, GTP-bound α-subunit and the $\beta\gamma$-subunit complex separately. Under in vitro conditions, the dissociated transducin subunits leave the membrane, due to a concentration-dependent equilibrium (*17, 42*). The release of the transducin subunits from the supported membrane should be easily detectable by surface plasmon resonance. Since under the chosen experimental conditions reactions occur in a defined geometrical arrangement, it might be also possible to investigate lateral diffusion of G proteins at the membrane surface and its modulation by the density of receptors in the membrane.

On SiO_2 supports, lithographically patterned grids of photoresist, aluminum oxide, or gold have been used to confine micrometer-scale patches of fluid membranes (*43*). On gold, a pattern of sulfur-bearing molecules of contrasting

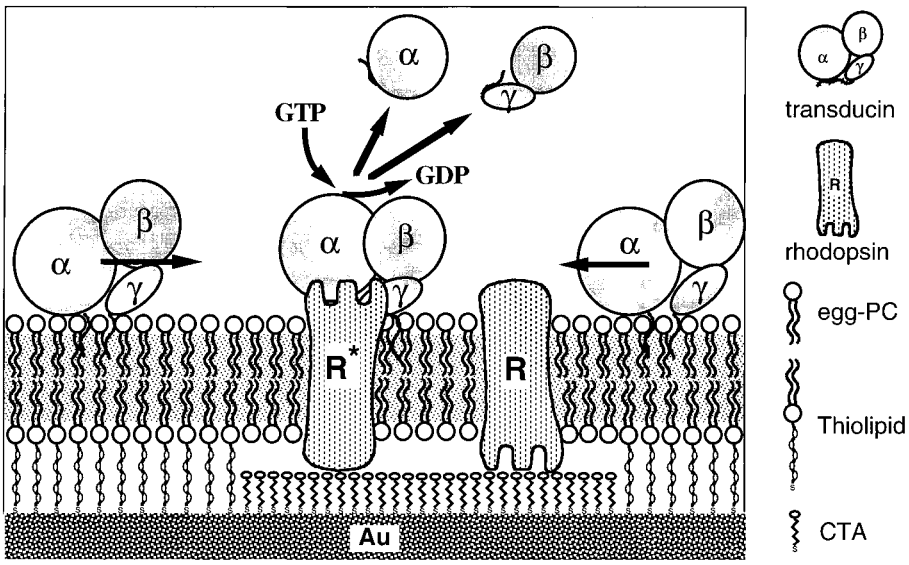

FIGURE 1: Schematic illustration of rhodopsin−transducin coupling on patterned supported membranes following a light flash. A gold surface (Au) serves as support for the membranes. It is functionalized with a patterned organic monolayer, consisting of alternating regions of carboxyl-exposing thiols (CTA, center) and regions of hydrocarbon-exposing thiolipids (left and right). Rhodopsin (R) and phospholipids (egg-PC) are self-assembled onto this structured support, forming membranes which alternate between phospholipid bilayer domains (on CTA) and monolayer domains (on thiolipids). Rhodopsin is preferentially present in the bilayer domains and active when incorporated in a transmembrane form, while transducin heterotrimers ($\alpha\beta\gamma$) bind to the surface of both mono- and bilayer regions of the membrane. Illumination of the membrane results in a pattern of rhodopsin activity, because rhodopsin−transducin coupling occurs only in bilayer domains. In addition, coupling requires a correct orientation of active rhodopsin (R*). It leads to nucleotide exchange (GDP → GTP) on the transducin α-subunit, dissociation of the α-subunit from the $\beta\gamma$-complex and their release from the membrane. Consequently, transducin is depleted in bilayer regions, but not in monolayer regions, which results in a lateral gradient of membrane-bound transducin. Transducin diffuses along this gradient from monolayer to bilayer domains. Such lateral displacement of protein mass and its release from defined locations on the membrane can be observed by one-dimensional imaging SPR.

properties serves the same purpose. Several different techniques are reported for patterning thiol layers on gold surfaces: Microcontact printing or micromachining (*44*), deep-UV photolithography (*45*), or Langmuir−Blodgett transfer of phase-separated thiolipid monolayers (*46*). For this work, we chose UV-lithography, because different pattern geometries can be easily realized with micrometer resolution (*47*).

Molecularly patterned organic layers on gold and silver surfaces have been investigated by SPR microscopy (*48*) and applied to antigen−antibody (*49*) and biotin−streptavidin binding (*50*). We have extended the "classical" SPR technique in a way similar to that of Hickel and Knoll (*51*) in order to simultaneously measure the activity of a 2D pattern of rhodopsin in supported membranes with high lateral and time resolution (one-dimensional imaging SPR, 1D-SPR). Rhodopsin activity was monitored by imaging the dissociation of transducin subunits from the activated rhodopsin−transducin complex. This was done on adjacent regions of a supported membrane with laterally varying rhodopsin density, which we intend to use for the observation of lateral transducin diffusion.

Each reaction step, starting from the creation of the 2D patterns up to the photoactivated dissociation processes of the G protein, was monitored simultaneously in detail on different regions of the patterned surface: assembly of rhodopsin membranes, and binding of transducin and its activation by photoexcited rhodopsin. For the formation of 2D patterns of functionally active rhodopsin, the gold surface was coated with a patterned monolayer of carboxy-functionalized thiols, forming hydrophilic, negatively charged regions (*52*), and thiolipids, forming tethered lipid monolayer regions (*32*). The aim of this procedure is to create continuous phospholipid membranes with alternating mono- and bilayer structures and, consequently, a laterally patterned distribution of active membrane proteins. We could demonstrate that for pure lipid membranes, such structures are indeed formed. Rhodopsin is readily incorporated in such membranes and remains fully functional. The surface pattern leads to a pattern of rhodopsin activity in the supported membranes, consistent with the idea that lipid bilayer structures occur predominantly on the hydrophilic parts of the surface. This combination of techniques is very promising for the investigation of lateral diffusion of transducin and can be extended to include signalling proteins downstream of the G protein.

We believe that an important application of our method for the measurement of activated GPCRs in micropatterned supported membranes is in the field of high-throughput screening for new therapeutic substances using libraries of compounds obtained from combinatorial chemistry and biotechnology. The rapid development of synthetic combinatorial chemistry on solid supports has already lead to promising novel concepts of spatially addressed synthesis and analysis (*53*, *54*). Our method opens the way for functional screening of activated membrane-bound receptors, in particular GPCRs.

EXPERIMENTAL PROCEDURES

Materials

Reagents. Solvents were purchased from Fluka, Switzerland, in the best available quality. Octyl glucoside (OG) was from Alexis Corp. Egg phosphatidylcholine (egg-PC)

was obtained from Fluka, Switzerland, and dissolved in chloroform and stored at −20 °C. Guanosine 5′-triphosphate (GTP) was purchased from Boehringer, Germany, and dissolved in buffer G to a 20 mM stock solution and stored at −20 °C.

Buffers. Buffer R consisted of 150 mM NaCl, 1 mM $MgCl_2$, and 10 mM sodium-phosphate, pH 7.0; buffer G was 100 mM NaCl, 1 mM $MgCl_2$, 1 mM DTT, 0.2 mM EDTA, and 10 mM HEPES, pH 7.4 (DTT and EDTA added immediately before use).

Synthesis of Compounds for Gold Functionalization: 11-Mercaptoundecanoic acid (CTA) was synthesized following standard procedures by bromide substitution via the isothiuronium salt (*55*).

Thiolipid [N-(14′-Mercapto-1′,11′-dioxo-3′,6′,9′-trioxa-12′-azatetradecyl)-2-oleoyl-1-palmitoyl-sn-glycero-3-phosphatidylethanolamine; See Figure 2B]. Commercially available 3,6,9-trioxaundecandioic acid was used to create the hydrophilic spacer between the natural phosphatidylethanolamine and the cysteamine. Desymmetrization was achieved by anhydride formation [1.2 equiv of DCC, CH_2Cl_2, r.t. for 12 h, filtration and concentration (*56*)] and coupling to *S*-dimethoxytrityl-protected cysteamine [0.8 equiv, 1 equiv of TEA, CH_2Cl_2, r.t. for 24 h, followed by flash chromatography, 75% yield (*57*)]. The free acid was activated (1.2 equiv of NHS, 1.2 equiv of DCC, CH_2Cl_2, r.t., 5 h, filtered and concentrated) and coupled with POPE (0.7 equiv, 1.5 equiv of DIEA, $CHCl_3$/iPrOH 4:1, r.t., 20 h, then flash chromatography, 60% yield). Finally, the acidic deprotection was accomplished with 5% TFA in CH_2Cl_2 in the presence of Et_3SiH (r.t., 2 h). The thiolipid was precipitated with acetonitrile, centrifuged, redissolved in $CHCl_3$, and washed with Na-EDTA, pH 7.4. Drying and evaporation gave the desired thiolipid in 81% yield: ^{1}H-NMR ($CDCl_3$/CD_3OD 4:1, 200 MHz) δ 7.83 (tm, 2H, NH), 5.32 (m, 2H, $CH_2-CH{=}CH-CH_2$), 5.18 (m, 1H, H-C(2)), 4.33, 4.16 (2dd, J = 12, 3.5 and J = 12, 6.5, 2H, H-C(1)), 4.08, 4.06 (2s, 4H, H-C(2′,10′)), 3.95−3.70 (5, 4H, CH_2OPOCH_2), 3.70 (br s, 8H, H-C(4′,5′,7′,8′)), 3.5−3.4 (m, 4H, N-CH_2), 2.66 (t, J = 6.5, 2H, -S-CH_2), 2.29 (dt, J = 7.5, 2.5, 4H, CH_2CH_2CO), 1.99 (m, 4H, $CH_2-CH{=}CH-CH_2$), 1.58 (m, 4H, CH_2CH_2-CO), 1.24 (br s, 32 H, $CH_{2-\text{fatty acid}}$), 0.86 (t, J = 6.5, 6H, $CH_{3-\text{fatty acid}}$); ^{13}C-NMR ($CDCl_3$/CD_3OD 4:1, 50 MHz) δ 174.0, 173.8, 171.2, 171.0, 129.8, 129.5, 70.3, 70.3, 70.2, 70.1, 63.7, 63.7, 63.5, 63.5, 62.9, 42.3, 40.0, 34.5, 32.1, 29.9, 29.7, 29.6, 29.4, 27.0, 25.1, 24.1, 22.9, 14.0; MS (ESI) 982.0 (M^+).

Protein Purification. Rhodopsin was solubilized in OG and purified over concanavalin A−Sepharose following the procedure of de Grip (*58*). Purified rhodopsin was eluted from the column with 200 mM α-methyl D-mannoside in 1.5% w/v OG, 10 mM BTP (pH 7.0), 130 mM NaCl, and 1 mM $MgCl_2$. Transducin was prepared as described (*18*) and stored in 10 mM BTP (pH 7.5), 100 mM NaCl, 0.5 mM $MgCl_2$, 0.2 mM EDTA, and 5 mM DTT. Rhodopsin stocks were diluted, if necessary, with 50 mM OG in buffer R, transducin stocks with buffer G.

Methods

Preparation of Monolayer-Covered Gold Substrates. Gold films of 54 nm thickness were evaporated onto SF 10 glass slides, covered by a 1 nm chromium adhesion layer. Immediately, the gilded slides were immersed in a 0.2 mg/mL (=0.9 mM) ethanolic solution of CTA (for experiments with pure CTA or structured CTA/thiolipid surfaces) or in a 0.1 mg/mL (=0.1 mM) solution of thiolipid in 50 mM OG (for experiments with pure thiolipid surfaces), respectively. Self-assembly of CTA was continued for at least 16 h, that of thiolipid for at least 24 h, to allow formation of a densely packed monolayer on the gold surface (*31, 32*). Directly before mounting on the cuvette, substrates were cleaned by rinsing with solvents and sonification in a bath sonificator (Sonorex PK, Model 102p) to remove unbound molecules. CTA surfaces were washed with ethanol (rinse, 1 min sonification, rinse). Thiolipid surfaces were cleaned both with detergent (rinse with water, 1 min sonification in 50 mM OG solution, rinse with water) and with solvents [rinse with ethanol, sonification in ethanol/hexane 1:1 (v/v), rinse with ethanol]. Substrates were dried in a nitrogen stream before further processing.

Photolithographic Structuration Process (Figure 2A). Structures were prepared by a UV lithography method similar to that of Tarlov et al. (*45*). This method yields patterns of very pure (*45*) and densely covered regions (*50*). A mask was placed directly on a dry CTA surface. The sample was illuminated for 1 h in air at 3 cm distance by a pen-ray mercury−argon lamp (Model 6035, Oriel Corp., Stratford, CT), which has pronounced UV lines below 200 nm. The lamp was shielded in a homemade housing which reached down to the substrate surface and was connected to a suction pump, in order to prevent damaging the mask-protected regions by the ozone produced. Photooxidation products (*59*) of CTA in illuminated regions were removed by 1 min sonification in water, followed by rinsing with water and ethanol, which revealed a bare gold surface. These regions were filled by a thiolipid monolayer using a self-assembly and washing process as for pure thiolipid surfaces (see above).

Line masks of different spacing were used to produce the patterns: either laser-cut steel masks with 140 μm or 70 μm wide lines, respectively, at 500 μm spacing; or copper grids for electron microscopy with 300 lines/inch (spacing 85 μm).

The quality of patterned surfaces from CTA/thiolipid was assessed by measurements of wetting, surface charge, and molecular composition (data not shown). CTA regions were hydrophilic (water contact angles 10−20°), remained covered by a water film when the sample was exposed briefly to air in 1D-SPR, and were negatively charged (as shown by polylysine binding). Thiolipid regions were hydrophobic (contact angles >90°) and broke the water film when exposed to air. Information about the molecular composition of the different regions was obtained from TOF-SIMS measurements. It was found that the regions were homogeneously covered and >95% pure (both CTA and thiolipid) in most cases.

Formation of Supported Membranes. Membranes were formed on the monolayer-covered gold surface by the micelle dilution technique (*32*). All manipulations were done in dim red light (Schott RG 665 filter) to avoid rhodopsin excitation. Egg-PC was used as the membrane lipid mixture. Micellar solutions were produced by dissolving a dried film of 1 mg of egg-PC in 1 mL of 50 mM OG in buffer R (=1.3 mM lipid), adding solubilized rhodopsin, and diluting with 50

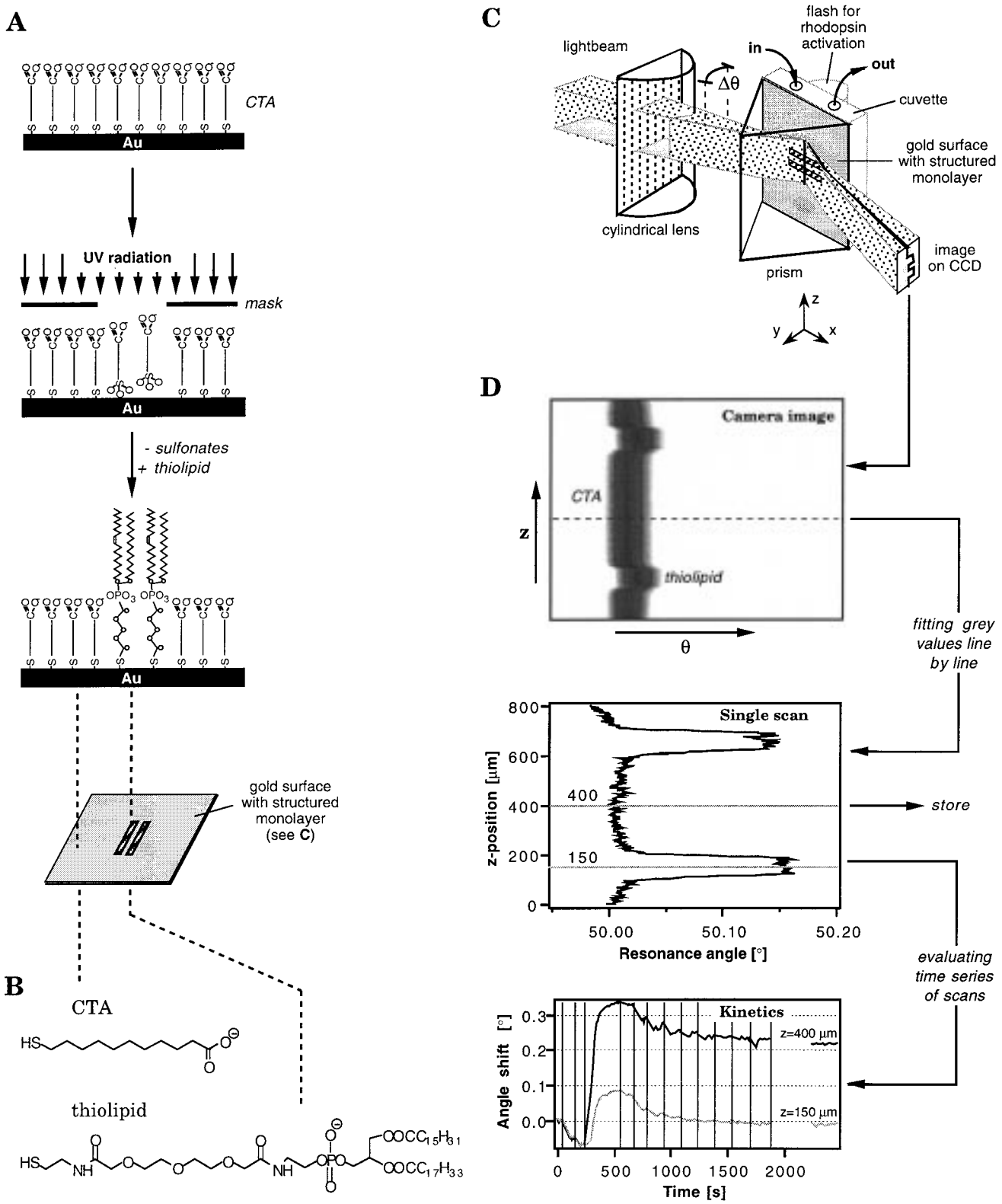

FIGURE 2: Preparation of structured surfaces (A, B) and the principle of SPR measurement (C, D). (A) Structuration process. A surface exposing a closed layer of carboxyl groups is prepared by self-assembly of CTA [see (B) for chemical structure] onto a fresh gold surface on a glass support. This monolayer is exposed to short-wavelength ultraviolet light through a mask. In the unprotected regions, thiols become photooxidized to sulfonates, which are removed by washing, revealing the gold surface. In a second self-assembly step, a monolayer of thiolipids [see (B) for chemical structure] forms in these regions. The pattern of the mask is thus imprinted on the gold surface in the form of a pattern of thiolipids and carboxythiols. (C) Optical configuration. A glass slide carrying the gold film with the patterned monolayer is assembled on the base of a 60° SF 10 prism via an index-matching oil. The CTA/thiolipid line pattern is oriented horizontally, i.e., parallel to the direction of the incoming lightbeam. This assembly is mounted on a stirred Teflon fluid cell, forming a cuvette of 200 μL volume. The modified gold surface contacts the sample solution. On the opposite side of the cuvette, a glass window allows for flash illumination of the surface. A cylindrical lens ($f = 40$ mm) focuses collimated, p-polarized light of $\lambda = 750$ nm through the prism onto the gold film, yielding a vertical focal line. The focal line is centered in the $x-z$ plane with respect to the surface pattern and defines the area

mM OG in buffer R to final concentrations of 0.32 mM egg-PC, 3.3 μM rhodopsin in 50 mM OG in buffer R (protein: lipid ratio 1:100). For experiments without rhodopsin, lipid concentrations of 0.32 or 1.3 mM egg-PC in 50 mM OG in buffer R were employed.

The sample was assembled with the Teflon half-cuvette, and after optical adjustments and calibration the surface was washed with methanol and water. The 200 μL cuvette was completely filled with buffer R, and the base line was recorded. Then, buffer was exchanged with the 200 μL micellar solution. From then on, the area of observation on the gold surface was always kept immersed in solution; any contact with air which might disrupt the membrane was avoided. The system was allowed to equilibrate, while continuously stirring the solution and measuring. For pure lipid layers, a stable state was reached within minutes, whereas in the presence of rhodopsin slow adsorption to CTA occurred, taking 20−60 min to completion. In some experiments with rhodopsin, the solution in the cuvette was subsequently diluted with 3 cuvette volumes of 0.32 mM egg-PC in 50 mM OG in buffer R to remove rhodopsin from solution and thus prevent possible rhodopsin aggregation on the surface during the following dilution step. Finally, membrane formation was initiated by slowly diluting the micellar solution with buffer, which led to self-assembly of lipids or lipids and rhodopsin on the surface. This dilution was done either manually, by stepwise injection of 0.5 or 1 cuvette volume of buffer R, respectively, using a syringe (4 times dilution 1:1.5, then 8 times 1:2), or by a peristaltic pump (initial flow rate 40 μL/min, after membrane formation 200 μL/min for 5 min). During dilution, the solution was continuously stirred. In some experiments, the freshly formed membrane was subjected to pulses of 10 mM OG/1 M NaCl in 10 mM phosphate buffer, pH 7, or to 1 M urea in buffer R to remove adsorbed vesicles.

Transducin Binding and Rhodopsin Activation. After membrane formation, buffer R in the cuvette was exchanged with buffer G, which resulted in a minimal change in resonance angles. The cuvette was continuously stirred. For determination of transducin membrane binding, 30 μL aliquots of transducin solutions of increasing concentration were injected consecutively into the cuvette. Between injections, binding was allowed to go to completion (at least 5 min). For other experiments, 40 μL of a 13 μM transducin solution was injected into the cuvette (final concentration 2.6 μM), unless specified otherwise.

The observed angle shifts directly reflect the amount of membrane binding of transducin, since bulk refractive index changes due to transducin stay below the resolution limit. Binding data were fitted by a modified Langmuir model, taking into account cooperative binding (*60*):

$$\frac{\Theta}{1-\Theta} = Kc \exp(\beta\Theta)$$

where $\Theta = \theta/\theta_{sat}$ is the fraction of occupied binding sites (the ratio of angle shift caused by bound transducin and angle shift at complete saturation), K is the Langmuir adsorption constant, c the transducin concentration in solution, and β the cooperativity coefficient. θ was determined experimentally as a function of c; free parameters of the fit are θ_{sat}, K, and β.

After transducin binding to the membrane was complete, the experiment was continued by photoexcitation of rhodopsin and transducin activation in the presence of GTP. A photo flash with a 530 nm cutoff filter (Schott OG 530) was used. GTP was added by injecting 20 μL of a GTP solution of 10 times the final sample concentration (final concentrations 1, 5, 10, or 2000 μM). In some experiments, a second light flash was applied later to estimate the efficiency of photobleaching. At the end of an experiment, 2 mM GTP was injected, and the cuvette was extensively rinsed with buffer G (>10 cuvette volumes) to determine the amount of irreversibly bound transducin. Experiments were performed at $T = 25$ °C.

Laterally and Time-Resolved Surface Plasmon Resonance Measurements (1D-SPR; Figure 2C,D). Measurements were performed on a homemade setup working in the Kretschmann configuration, using an extension of the technique developed by Hickel and Knoll (*51*). Optical components were from Spindler & Hoyer, Göttingen, Germany, and mechanical components from Physik Instrumente, Waldbronn, Germany, and Newport, Zurich, Switzerland. The optical configuration is depicted in Figure 2C. A 150 W xenon arc lamp (Osram, München, Germany; housing and power supply from Müller, Moosinning, Germany) served as light source. The beam was collimated by a lens−pinhole−lens arrangement (beam diameter 10 mm). An interference filter (Laser Components, Olching, Germany; half-bandwidth 13 nm) selected the measuring wavelength of 750 nm, which was used instead of the more common 633 nm in order to avoid any excitation of rhodopsin. Beam homogeneity was checked by scans with s-polarized light. The CCD camera (Model C3077) was from Hamamatsu, Hertfordshire, England. For experiments on pure (unstructured) surfaces, the reflected light was directly collected by a linear diode array detector (Hamamatsu C4350) instead of the camera.

At defined time intervals, a camera image was grabbed (frame grabber card Pulsar, Matrox Ltd., Quebec, Canada, with 10 bit A/D converter and adjustable gain) and processed

of observation. The reflected wedge-shaped light beam is passed through imaging and magnification optics made from two crossed cylindrical lenses (not shown) and directed onto a CCD camera. Both prism and camera are mounted on turntables, usually set to angles of 51° (prism tip) and 102° with respect to the incident light. The focal sector defines the range of incidence angles $\Delta\theta$ around the beam center at 51°. The plasmon resonance is observed as a dark line in the reflected light at the resonance angle. At defined time intervals, a camera image is grabbed and analyzed. (D) Image analysis. The recorded image (top) represents the intensity of the reflected light, given by gray values, vs angle (corresponding to a conventional angle-scanning SPR resonance curve) vs position in the sample z-direction. Within the range of incidence angles $\Delta\theta$, the angle of plasmon resonance at a given z-position is marked by a minimum in the reflected light intensity. This resonance angle is calculated on-line for each z-position by a parabolic fit to the resonance curve (given by the horizontal camera line at the respective z-position). Combining the resonance angles vs z-positions yields a single scan (middle). Thiolipid regions on a structured surface exhibit a resonance angle shifted by 0.15° with respect to CTA regions. From a time series of single scans, the evolution of the resonance angles for selected regions of the surface is traced, represented in an "Angle shift" vs "Time" graph ("Kinetics", bottom). Angle shifts are relative to resonance angles at time = 0 (displayed here for two selected z-positions vs time).

on-line with software developed in our laboratory (Figure 2D). Each image covered a vertical distance of approximately 800 μm on the sample. The intensity values of each of the 480 horizontal camera lines correspond to a resonance curve for the respective *z*-position. From these values, the angular position of the respective resonance minimum was first estimated and then refined by a parabolic fit to that part of the resonance curve surrounding the estimated position. This time-consuming, but very reliable, fitting procedure limited the time resolution to 3 scans per second. The photo flash for rhodopsin activation was also computer-controlled, so that frame-grabbing could be synchronized with it.

The lateral resolution was limited in the *x*-direction by the width of the focal line (approximately 0.5 mm), necessitating the use of horizontally aligned line patterns (so as not to integrate over two different surface regions). In the *z*-direction, the limit of the resolution was given by the lateral decay length of surface plasmons, which is 15 μm for a gold−water interface at $\lambda = 750$ nm [calculated from ref (*61*)]. The angular resolution given by camera and evaluation software was 2/1000°. Fresnel calculations of the resonance angle shift at $\lambda = 750$ nm caused by lipid membranes ($n = 1.45$) yielded a relation of 11.8 Å average film thickness per 0.1° angle shift. This corresponds to a resolution limit of 0.2 Å for a lipid membrane.

To calculate the geometrical thickness (Δd) of an adsorbed organic layer from the angle shift, the refractive index (n_{layer}) of the respective material must be used as an input parameter. For organic layers which are thin with respect to the light wavelength, the angle shift $\Delta\theta$ is proportional to the change in optical thickness: $\Delta n \times \Delta d$ ($\Delta n = n_{layer} - n_{buffer}$). This is also a measure of the adsorbed mass density on the gold surface. Taking literature values, we used $n_{layer} = 1.5$ for densely packed thiol layers on gold (*62*) and $n_{layer} = 1.45$ for phospholipid membranes (*32*, *63*) and proteins adsorbed at the organic interface (*64*−*66*).

At the beginning of a measurement, the setup was calibrated by a scan first in water, and then in a 1 M NaCl solution. The "standard" angle shift caused by the refractive index difference of the two liquids was used to convert camera pixel to angle scales.

During each measurement, the quality of the (coated) surface was checked by monitoring the values for minimum intensity and half-width of the scans. The minimum intensity was always below 10% of the maximal intensity of the reflected light, the half-width was smaller than 2°, and its maximal increase during an experiment was 10%.

RESULTS

Structured Functionalized Gold Surfaces. As a support for patterned membranes, surfaces with well-controlled, laterally varying interfacial properties were constructed using thiol−gold chemistry (*31*), as described under Experimental Procedures and in the legend of Figure 2. The structured support consisted of monolayers of CTA and thiolipid, each separately self-assembled on the gold film into laterally patterned domains (Figure 2).

In 1D-SPR, these structured surfaces revealed a regular pattern of resonance angles (Figure 3A,C, "surface") and consequently of mass density. For thiolipid regions, the resonance angle was shifted by 0.140° ± 0.016° (8 independent preparations) with respect to CTA regions. Theoretically, an angle difference of 0.15° is expected between densely packed thiolipid and CTA monolayers. This is calculated from the molecular area of 50 Å^2 for thiolipid measured on the film balance (data not shown) and published parameters for a hydroxythiol layer [molecular area 22 Å^2, layer thickness 13 Å, refractive index $n = 1.5$ (*62*)].

The borders between adjacent CTA and thiolipid regions appeared blurred in 1D-SPR (Figure 3A): They looked like continuous transitions from one region to the other. When EM-grids were used as masks, the width of this transition region in SPR scans ranged from 13 to 19 μm. This corresponds almost exactly to the lateral decay length of the plasmons (15 μm) which indicates that the real transition zone between regions might be much narrower. TOF-SIMS revealed that its width was actually less than 1 μm.

Phospholipid Membrane Self-Assembly. Experiments with pure lipid membranes (without rhodopsin) proved the feasibility of forming a regular pattern of adjacent lipid mono- and bilayers on a complementary patterned surface, which served as a template.

The result of a typical experiment is shown in Figure 3A,B: A patterned CTA−thiolipid surface was incubated with a solution of mixed lipid/detergent micelles, which was subsequently diluted below the CMC. By comparing the SPR scans of the washed surface in buffer ("surface", Figure 3A) and the surface after micelle injection and dilution ("membrane", Figure 3A), it becomes clear that the phospholipids fill up the surface structure. However, structure boundaries can still be recognized. The high CMC of OG facilitates its removal, so the extensively washed membranes are essentially detergent-free. Mean angle shifts for egg-PC membranes on structured surfaces were 0.40 ± 0.006° on CTA regions, corresponding to a thickness of 47 Å, and 0.22 ± 0.021° on thiolipid regions, corresponding to a thickness of 26 Å (3 experiments each). The angle shifts obtained did not depend on dilution speed, nor on dilution procedure. On a pure CTA surface, egg-PC bilayer formation was associated with an angle shift of 0.46°.

Figure 3B shows the kinetics of membrane formation at different positions of the surface. Injection of the micellar solution caused angle shifts of 0.20° ± 0.01° on CTA and 0.28° ± 0.02° on thiolipid (3 experiments). Two effects contribute to these angle shifts: the increased refractive index of the solution and surface binding. The 50% bigger angle shift on thiolipid suggests that in detergent solution the hydrophobic surface is already covered by an adsorbed detergent/lipid layer. Upon dilution, the refractive index dropped, causing a lowering of resonance angles; 180 s after the onset of dilution, the resonance angles increased quickly, especially pronounced for CTA regions. At this point, the OG concentration in the cuvette was 27 mM, close to the critical micelle concentration (CMC) of pure OG (25 mM). Finally, after extensive washing (>10 cuvette volumes), stable membranes were established.

Rhodopsin-Containing Membranes. Membranes of egg-PC and rhodopsin ("rhodopsin membranes") were formed simply by including rhodopsin in the lipid/detergent mixed micelles. An example is shown in Figure 3C,D. The basic surface structure was reproduced very clearly in the rhodop-

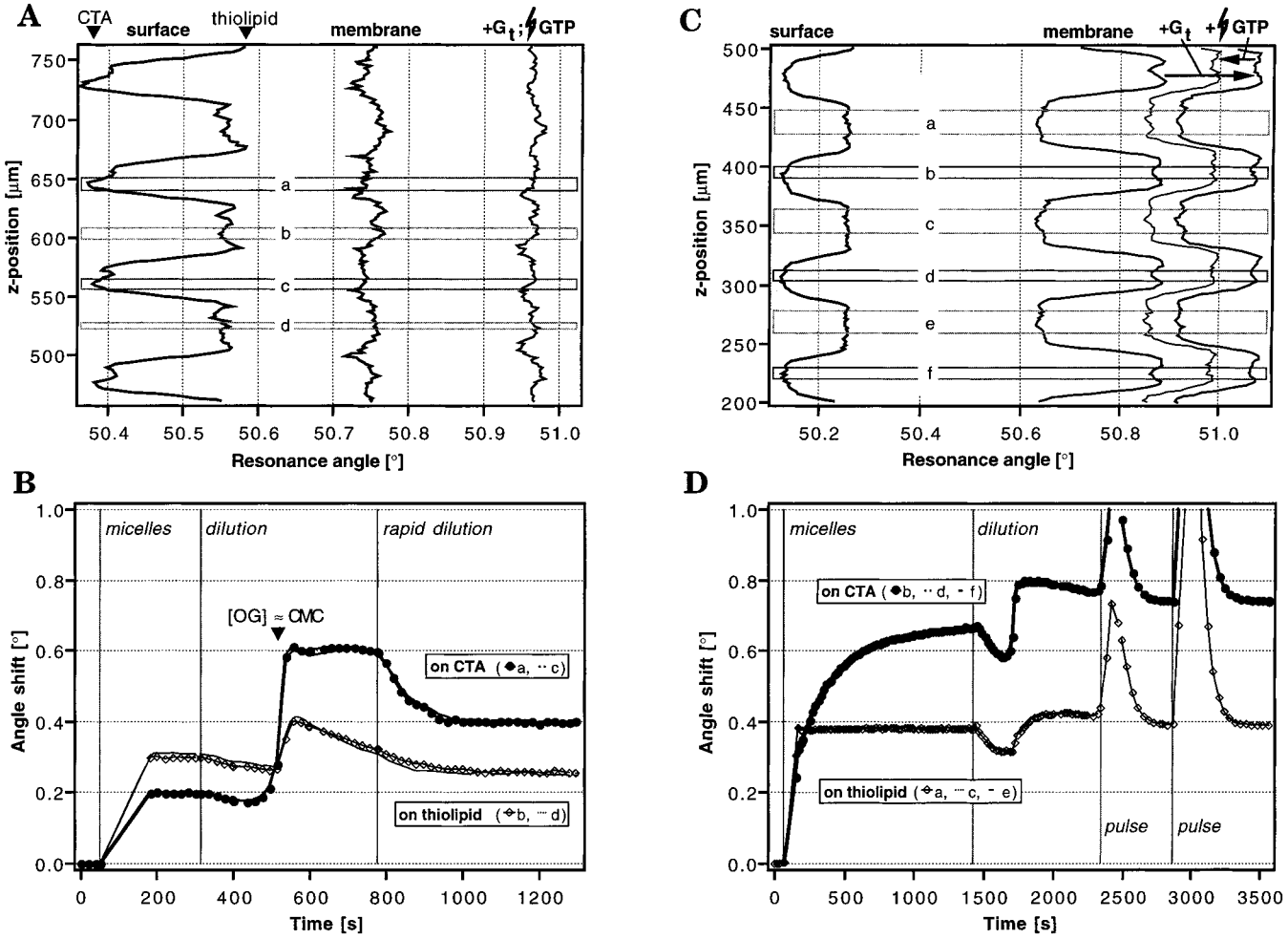

FIGURE 3: Formation of supported membranes on structured surfaces, without rhodopsin (A, B) and with rhodopsin (C, D) as observed by imaging SPR. (A) SPR scans (resonance angle vs *z*-position) of a gold surface coated with a CTA/thiolipid patterned monolayer (85 μm-spaced stripes) at different stages of the experiment. Letters a to d denote the surface regions for which the reaction kinetics are evaluated in (B). The experiment begins with the solvent-washed surface ("surface"). The scan shows angle maxima for the thiolipid regions (e.g., b, d) and minima for the CTA regions (e.g., a, c) on the surface. A pure lipid membrane is formed on this surface by micelle dilution ("membrane"). At this step, the surface is homogeneously covered (equal mass density for CTA + phospholipid bilayer and for thiolipid + phospholipid monolayer). Transducin is then injected into the cuvette (final concentration 3 μM) and binds homogeneously to the lipid membrane ("+G_t", angle shifts 0.22° on CTA, 0.21° on thiolipid). 5 μM GTP and a flash applied to the system have no further effect. (B) Kinetics of lipid membrane formation on CTA [filled circles correspond to region a in (A); thick line to region c] and thiolipid (open diamonds, region b: line, region d) regions. The washed surface (time = 0) is the reference for angle shifts. Mixed lipid/detergent micelles are injected into the cuvette ("micelles", time = 50 s), resulting in an increase in angles (0.21° on CTA, 0.31° on thiolipid) due to the different refractive index of the solution and to detergent binding to the thiolipid surface (note, that in the time interval between 50 and 200 s no intensities were measured due to manipulations at the cuvette). After equilibration, dilution of the micelles is begun ("dilution", time = 320 s). At time = 480 s, the concentration of detergent drops below the CMC. The jump in the signals indicates spontaneous lipid membrane formation on the surface, more pronounced on CTA than on thiolipid. Finally, the detergent and lipid vesicles formed in the process are completely removed from the cuvette ("rapid dilution"), the resonance angles stay constant, and a stable membrane has formed. The final values of the angle shifts (0.40° on CTA, 0.24° on thiolipid) are in accordance with a lipid bilayer on CTA regions and a monolayer on thiolipid regions. Note the good agreement of the kinetics taken from different spots at the surface (comparing a and c, b and d). (C) SPR scans from an experiment similar to (A), but with rhodopsin in the membrane. Although the same type of surface was employed ("surface"), the rhodopsin/lipid membrane ("membrane") is characterized by larger angle shifts than the pure lipid membrane in (A), especially in the CTA regions (b, d, f). Transducin binding ("+G_t", 3 μM) is now more pronounced to the membrane on thiolipid regions (0.26°) than on CTA regions (0.21°). A flash applied after addition of 5 μM GTP ("GTP") to the cuvette leads to transducin desorption from the membrane due to the rhodopsin activity. (D) Kinetics of lipid/rhodopsin membrane formation on CTA (b, filled circles; d, f, thick lines) and thiolipid (a, open diamonds; c, e, lines) regions. At time = 150 s, mixed lipid/rhodopsin/detergent micelles are injected into the cuvette ("micelles"). Unlike in (B), slow adsorption kinetics can be observed on CTA, but not on thiolipid. Angle shifts due to micelle injection and adsorption are 0.67° on CTA, 0.38° on thiolipid, both higher than for pure lipid/detergent micelles in (B). At time = 1430 s, dilution is started ("dilution"). At time = 1800 s, a signal jump indicates the transition from detergent micelles to membrane assembly, passing the detergent CMC. When the concentration of detergent is low, two pulses of buffered 1 M NaCl/10 mM octyl glucoside are applied ("pulse") to remove membrane-adsorbed vesicles. The final values of the angle shifts (0.74° on CTA, 0.39° on thiolipid) are considerably higher than for the pure lipid membrane in (B).

sin membrane: much more material adsorbed to CTA regions than to thiolipid regions.

(i) On CTA. Rhodopsin membranes were generally thicker than pure lipid membranes. They were associated with an SPR angle shift of 0.57° ± 0.11° on CTA, corresponding to 67 Å average thickness (7 experiments).

An upper limit for the density of incorporated rhodopsin can be estimated by comparing this angle shift with that of

pure lipid membranes (0.40°). If the surplus in membrane mass (0.17°, which is 43% of a lipid bilayer) is attributed entirely to rhodopsin, this yields 1 rhodopsin/20 nm^2 (80 nmol/m^2). This calculation is based on the respective projection areas of rhodopsin [800 Å^2 (*9*, *14*)] and lipid molecules (60 Å^2) and their respective molecular masses.

A lower limit for the rhodopsin density in the supported membranes can be obtained from the amount of rhodopsin binding to the surface prior to dilution and membrane assembly. The kinetics of layer formation (Figure 3D) reveal slow adsorption of material to CTA directly after injection of rhodopsin-containing micelles, in contrast to pure lipid/detergent micelles (Figure 3B), which reached a stable state within seconds.[2] The angle shift due to incubation with rhodopsin-containing micelles on CTA regions was 0.54° ± 0.10°, which was 0.34° more than for micelles without rhodopsin. In rhodopsin/OG micelles, the mass ratio of detergent:protein is about 2:1 (*67*). A gross estimate of the angle shift due to adsorbed rhodopsin molecules would then be 0.11°, corresponding to 1 rhodopsin/30 nm^2 (57 nmol/m^2). Since the difference in angle shifts between rhodopsin membranes and pure lipid membranes (0.17°) is higher than the value attributed from rhodopsin alone (0.11°), additional lipid at the interface would then account for the remaining mass difference. Assuming identical lipid packing, rhodopsin membranes would have 15% additional effective bilayer area.

Two experimental approaches to enhance the contrast in rhodopsin density between CTA and thiolipid regions were tried: (i) washing of the nascent membrane with a high salt solution containing detergent below the CMC, and (ii) replacement of the rhodopsin/lipid/detergent micellar solution with a lipid/detergent micellar solution before dilution. These experimental steps should remove loosely bound rhodopsin from the membranes. The membranes turned out to be remarkably stable against washing with 1 M NaCl/10 mM OG (see Figure 3D: pulses have almost no effect), final angle shifts for membranes being 0.57° ± 0.17° with washing, the same value as stated above for membrane formation without washing. Washing with 1 M urea gave the same result. In contrast, replacement of rhodopsin micelles with egg-PC micelles before dilution yielded thinner membranes (angle shift 0.51° ± 0.03°). By stirring slowly during the egg-PC "wash", lateral gradients of rhodopsin membrane mass were obtained on the CTA regions of a patterned sample (Figure 7).

(ii) On Thiolipid. Rhodopsin membranes on thiolipid were associated with angle shifts of 0.32° ± 0.06°, corresponding to an average thickness of 38 Å (7 experiments). The 0.10° difference to pure lipid membranes gives the upper limit for the rhodopsin density on thiolipid as 1 rhodopsin/46 nm^2 (36 nmol/m^2).

On thiolipid regions, the angle shift caused by injection of the micellar solution (Figure 3D) was also higher than with pure lipid/detergent micelles (Figure 3B), though no kinetics of adsorption could be resolved. It amounted to 0.37° ± 0.01°, which is 0.08° more than without rhodopsin.

[2] In Figure 3B, no intensities were measured in the time interval between $t = 50$ s (time of injection of detergent micelles) and $t = 200$ s; however, we know from other measurements that detergent injection resulted in an immediate intensity change. Nevertheless, the time courses in Figure 3B for $t > 200$ s are clearly different from the rhodopsin adsorption kinetics in Figure 3D on CTA.

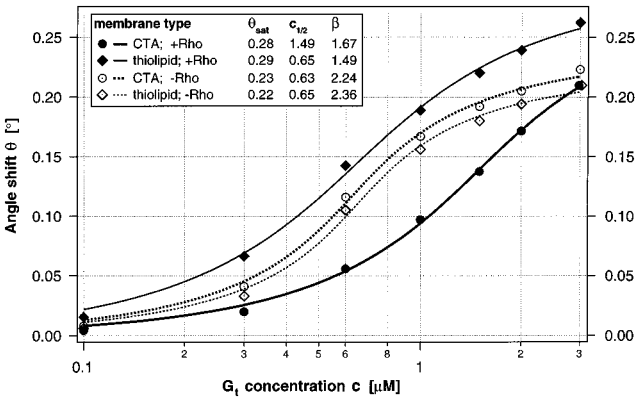

FIGURE 4: Dark binding of transducin to different supported membranes. The SPR angle shifts caused by transducin binding to membranes at different concentrations in solution are shown. The data were compiled from experiments with structured CTA/thiolipid surfaces. The binding to membranes containing rhodopsin (+Rho) is indicated by filled circles (CTA regions) and diamonds (thiolipid regions), and that to pure lipid membranes (−Rho) by open symbols. Fits are indicated by solid lines for rhodopsin membranes and dotted lines for lipid membranes. The data could not be fitted with a simple Langmuir isotherm, so possible cooperative effects of binding were taken into consideration using a modified Langmuir model (see Methods). Parameters of the fits are given in the box: saturation value of the angle shift θ_{sat}; transducin concentration at half-maximal binding $c_{1/2}$; cooperativity coefficient β. Saturation values and cooperativity coefficients are similar for membranes on CTA and thiolipid. Pure lipid membranes and rhodopsin membranes on thiolipid share the same $c_{1/2}$, but rhodopsin membranes on CTA have a markedly lower affinity for transducin. When fitting the data with a constant β of 1.5, qualitatively similar results were obtained (not shown).

The calculation of a rhodopsin density from this value is hindered by the unknown amount of stripping of detergent from the rhodopsin/OG micelles upon binding to the already detergent-covered thiolipid surface. A lower limit for rhodopsin density would be 1 rhodopsin/174 nm^2 (10 nmol/m^2, no stripping of OG), with 25% additional effective membrane area in lipid bilayer form.

Neither washing with 1 M NaCl/10 mM OG nor washing with 1 M urea changed the membrane thickness significantly (final angle shifts for the "washed" membranes on thiolipid: 0.33° ± 0.06°). Micelle replacement before dilution, however, yielded membranes of mass coverage similar to lipid monolayers (angle shifts 0.18° ± 0.02°).

Transducin Binding to Supported Membranes. Dark binding of transducin to patterned egg-PC membranes with and without rhodopsin was investigated for several reasons. First, the saturation density of transducin on the supported membranes is an important parameter for evaluating transducin binding and desorption kinetics. Second, dissociation constants were obtained and compared to those for disk membranes, allowing conclusions about the influence of lipid environment, structuration, and the presence of rhodopsin on transducin dark binding. Third, transducin binding was exploited as a probe of membrane properties when comparing the different membrane types.

Binding isotherms of transducin to supported egg-PC monolayers and to bilayers were very similar (Figure 4). To obtain a good fit to a Langmuir model, positive cooperativity of binding had to be included. This cooperativity was very pronounced for binding to pure lipid membranes (distinctly s-shaped plots). Transducin binding to egg-PC membranes

Table 1: Transducin Binding to Rhodopsin Membranes and Its Light-Induced Release

			surplus[c] membrane mass (%)				G_t binding[d] (deg)		G_t desorption[e] (%)		release rate constant, k_{obs} (s^{-1})	
no.	surface[a]	wash proc[b]	TL	CTA	$[G_t]$ (μM)	[GTP](μM)	TL	CTA	TL	CTA	TL	CTA
1	CTA	no	−	61	1.6	10	−	0.139	−	67		
2	TL	OG/salt	29	−	2.6	10	0.237	−	20	−		
3	CTA/TL	no	66	39	1.5	1	0.161	0.106	23	34	0.120	0.245
4	CTA/TL	no	59	52	2.6	10	0.227	0.176	37	47	0.193	2.416
5	CTA/TL	OG/salt	16	32	2.5	10	0.236	0.170	3	26	−[f]	2.245
6	CTA/TL	EPC	−11	18	2.6	5	0.242	0.136	17	30	0.162	1.386

[a] *CTA*, pure CTA surface; *TL*, pure thiolipid surface; *CTA*/*TL*, stripes of thiolipid in CTA surface. [b] *no*, membrane formation by simple dilution; *OG*/*salt*, pulse of buffered 10 mM octyl glucoside/1 M NaCl during dilution; *EPC*, exchange of mixed rhodopsin/lipid/detergent micellar solution by pure lipid/detergent micelles immediately before dilution. [c] Relative to pure lipid membranes (without rhodopsin): on CTA, 0.41°, on thiolipid, 0.22°. [d] Nonspecific G_t binding to pure lipid membrane on structured surface: CTA, 0.06°; thiolipid, 0.04° ($[G_t] = 3$ μM). [e] Amount of G_t dissociated from the membrane by activated rhodopsin relative to amount of G_t bound before. [f] Cannot be fitted accurately due to small amplitude.

saturated at 0.22−0.23°. This corresponds to 56% of a densely packed transducin monolayer, for which one would expect an angle shift of 0.39°, taking a transducin molecular area of 4000 Å^2 from ref (*68*). Part of this saturation value corresponded to irreversibly bound transducin, which amounted to angle shifts of 0.06° on CTA and 0.04° on thiolipid. The concentration at half-maximal binding ("dissociation constant") is 0.6 μM, in good agreement with the apparent dissociation constant of transducin measured in rod outer segment membranes [0.3 μM (*17*)].

The presence of rhodopsin increased the saturation values for transducin binding by about 25% on both surface types to $\Delta\theta \approx 0.28-0.29°$, corresponding to 1 transducin binding site per 56 nm^2. Transducin binding to rhodopsin membranes was little influenced by the mass of the membrane adsorbed to the support (Figure 7). For illuminated rhodopsin membranes, the amount of irreversibly bound transducin varied from 0.05° to 0.17° on CTA and from 0.03° to 0.16° on thiolipid, depending on the preparation. These values include any transducin which may stay bound to rhodopsin directly. The dissociation constant of transducin on thiolipid remained the same as for pure lipid membranes (0.6 μM), but was increased to 1.5 μM on CTA, when rhodopsin was incorporated in the membranes. At a concentration of 2.6 μM transducin, average surface densities of transducin were 1/87 nm^{-2} on CTA and 1/65 nm^{-2} on thiolipid. On pure surfaces, transducin binding to membranes was slightly increased with respect to that on structured surfaces (Table 1, lines 1 vs 3 and 2 vs 4, respectively).

Rhodopsin Activation: Typical Experiment. In the following, we describe a standard experiment for investigation of the light-induced coupling of rhodopsin and transducin on the supported membrane. Figure 5 shows the corresponding transients, data are summarized in Table 1, line 4. Once the rhodopsin membrane had been formed on the structured surface, the experimental protocol followed the sequence: transducin injection(s) → GTP addition → flash. After injection, transducin binding was observed by an increase of SPR resonance angles. GTP addition had hardly any effect, and the flash (at $t = 0$) immediately lead to a dissociation of transducin from the surface as reflected in a decrease of SPR resonance angles. Since in the experimental protocol the dissociation signal directly follows the flash, its time course can be precisely resolved. After dissociation of transducin, SPR resonance angles remained stable for some time, and then rebinding occurred.

These signals can be readily interpreted by analogy to light-scattering measurements on suspended rod outer segments (ROS) (*16*) or disk membranes reconstituted with transducin (*16, 17*). First, addition of transducin leads to membrane binding (*85*), which can be described by a Langmuir adsorption isotherm (see last section). Addition of GTP in the dark had no effect. The flash-induced dissociation results from the complete release of the G_α-subunit and a partial release of the $G_{\beta\gamma}$-subunit from the membrane (*17, 69, 85*), following rhodopsin-catalyzed dissociation of transducin heterotrimers (holo-G_t) into subunits. The conformational change of transducin which leads to dissociation of the heterotrimer into subunits is induced by GDP → GTP exchange on its α-subunit when in contact with correctly oriented rhodopsin in the active Meta II state (R*) [see, for example, ref (*7*)].

The following additional observations and control experiments confirm the above interpretation for the supported membranes: (1) Addition of GTP to the transducin-loaded membrane did not change the signal, indicating an unmeasurably low rhodopsin activity in the membrane before the flash. (2) Resonance angles decreased after the flash only when rhodopsin was incorporated in the membrane. A flash had no effect on a pure egg-PC membrane in the presence of transducin and GTP (negative control, Figure 3A). (3) Resonance angles did not change upon illumination of a rhodopsin membrane in the absence of transducin (data not shown). This confirms that the SPR dissociation signal corresponds exclusively to transducin release. (4) Transducin binding and release are reversible. Rebinding occurred and was reversed with a second GTP injection, but not with a second flash, which caused a small binding signal instead (Figure 5). Consequently, rebinding was not a result of a fast decrease in the amount of R*, but a result of a dropping GTP level due to GDP−GTP exchange and hydrolysis of GTP bound to α-subunits soon after the first flash. (5) Finally, in the absence of GTP, no release signals, but additional small binding signals, were observed following the flash (Figures 6 and 7). This has been observed also in light-scattering experiments under GTP-deficiency and was interpreted as 1:1 stoichiometric binding of holo-G_t to R* (*16, 17*), which was not released because of lack of GTP. If GTP was added subsequently, release signals were observed (Figure 6). This shows that rhodopsin, once exposed to light, stays active in the supported membranes during the time of the experiment.

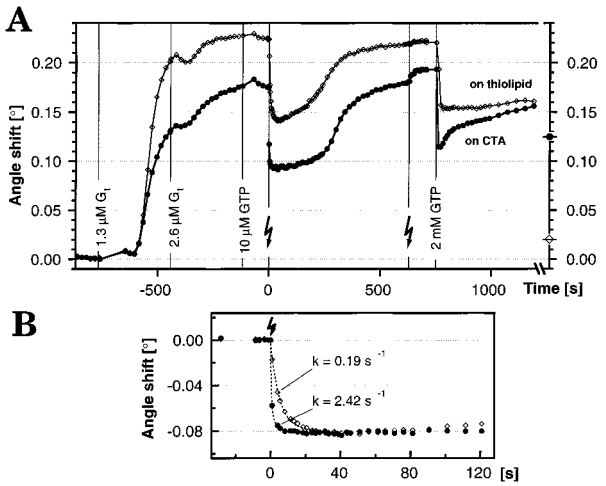

FIGURE 5: (A) Activation of rhodopsin in supported structured membranes. The kinetics of transducin binding to a rhodopsin membrane (thiolipid regions, open diamonds; CTA regions, filled circles) and its desorption upon flash photolysis of rhodopsin are shown. Two subsequent injections of transducin (G_t, final concentrations 1.3 and 2.6 μM) lead to angle shifts of 0.23° on thiolipid and 0.18° on CTA. At time = −100 s, GTP is injected. No angle shift is observed, indicating no dark activity of rhodopsin. At time = 0, a flash is applied, leading to transducin desorption with an amplitude of $\Delta\theta = -0.08°$. After a certain time, rebinding occurs. This is due to GTP being used up and to the decay of activated rhodopsin (see Results). A second flash applied at time = 630 s leads to slightly increased transducin binding, resulting from activation of more rhodopsin molecules and binding of transducin directly to them. At this time, nucleotide exchange and desorption are already reduced by the lack of GTP. This is changed by injection of GTP at high concentration (2 mM), followed by desorption of transducin. Rebinding on thiolipid is now much slower than after the first flash, but on CTA it proceeds quickly. This effect clearly does not result from lack of GTP. The symbols on the right axis indicate the values after extensive washing with buffer, i.e., the amount of irreversibly bound transducin. More transducin remains adsorbed on the rhodopsin membranes on CTA than on thiolipid, and irreversible binding of transducin increased with time (more transducin can be desorbed by the first flash than by the final buffer wash). A possible reason for this is rhodopsin decay, which may also be the reason for the lower dissociation signal following the second flash as compared to the first flash, in spite of a 200-fold increased GTP level. (B) Kinetics of desorption following the first flash. Data points were fitted (broken lines) by a single exponential (thiolipid region) and a double exponential (CTA region). In the latter case, the fast kinetics accounted for about 80% of the amplitude. The fast rate constants are given. Transducin desorption is 12 times faster in the CTA regions than in the thiolipid regions.

In the experiment depicted in Figure 5, the kinetics of desorption following the first flash differed by an order of magnitude between CTA and thiolipid regions. This is an indication of a higher density of active rhodopsin, R*, in membranes on CTA regions than on thiolipid regions. The absolute amplitudes of desorption following the first flash were the same on the whole surface (0.08°), but the relative desorption amplitudes were 37% of the amount of transducin bound before the flash on thiolipid and 47% on CTA. The dissociation amplitudes represent saturation levels because they are generally correlated neither with R* density nor with GTP concentration; therefore, they monitor the fraction of the total pool of transducin that interacts with R*, undergoes GDP/GTP exchange, and is finally released.

Rhodopsin Activation: Detailed Analysis. The activation of rhodopsin and transducin by a flash was also investigated by first applying the flash and injecting GTP afterward

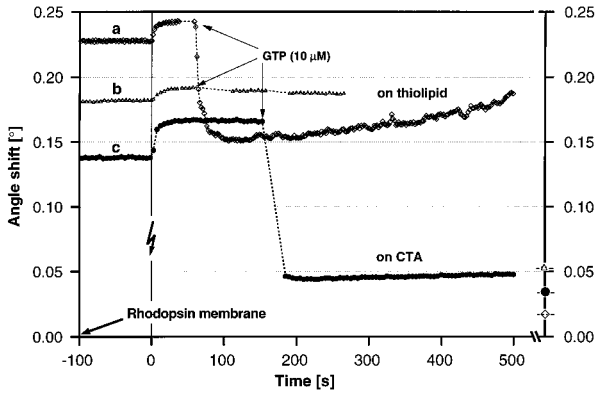

FIGURE 6: Activation of rhodopsin in supported membranes on pure (unstructured) surfaces. Two measurements on thiolipid surfaces (trace a, open diamonds; trace b, small triangles) and one on a CTA surface (trace c, filled circles) are shown. At time = −100 s, lipid/rhodopsin membranes have formed on the surfaces, and transducin is bound to them (transducin concentrations in solution are 2.6 μM for the experiments on thiolipid and 1.6 μM for the one on CTA). Angle shifts are relative to the lipid/rhodopsin membrane as zero line, so values at time = 0 correspond to the amount of bound transducin. At time = 0, a flash is applied, resulting in further transducin binding. This process is caused by rhodopsin binding transducin directly, thereby freeing binding places in the membrane, which are in turn filled by transducin molecules from solution. Addition of GTP leads to transducin desorption from both types of membranes (traces a and c), but in one case rhodopsin on a thiolipid surface was unable to activate transducin (trace b). The amount of irreversible transducin binding is indicated by the symbols on the right axis: it is highest for the membrane with the nonfunctional rhodopsin (trace b), and for the membranes with functional rhodopsin lower on a thiolipid support (trace a) than on CTA (trace c). Due to technical reasons, no intensities were recorded directly before GTP injection in trace a, and directly after GTP injection in traces b and c.

(Figure 6, sequence: transducin injection → flash → GTP). Binding signals upon flashing in the absence of GTP reflect stoichiometric binding of transducin to rhodopsin in the MII state and in the correct orientation (R*) (*16*). The amplitude of this binding signal is proportional to the density of R*. Three experiments of this kind on pure surfaces are shown in Figure 6, one on CTA and two on thiolipid surfaces. On CTA, the binding signal amounted to $\Delta\theta \approx 0.027°$, corresponding to 1 R* per 600 nm^2 (trace c). Generally, the density of active rhodopsin was remarkably independent of the mass of the membrane adsorbed on CTA. For example, in Figure 7 a $\Delta\theta$ of approximately 0.025° was measured as the amplitude of the binding signal for all CTA regions in spite of 50% variation in the mass of the membrane. On thiolipid, the amplitudes of the binding signals in Figure 6 were $\Delta\theta \approx 0.016°$ (1 R* per 1000 nm^2, trace a) and 0.010° (1 R* per 1500 nm^2, trace b). However, there were also experiments where no binding signal was seen on thiolipid regions, the R* density being too low to be detected.

Subsequent addition of GTP always led to transducin desorption from CTA regions (e.g., trace c). In Figure 6, virtually all reversibly bound transducin was released (two-thirds of the total bound transducin), indicating that (1) a saturating density of R* was present after the flash, and (2) all the dissociated transducin subunits left the membrane readily and completely.

On thiolipid regions, GTP-induced desorption was also observed in most cases (e.g., Figure 6, trace a). Sometimes, however, no such desorption signal could be seen (e.g.,

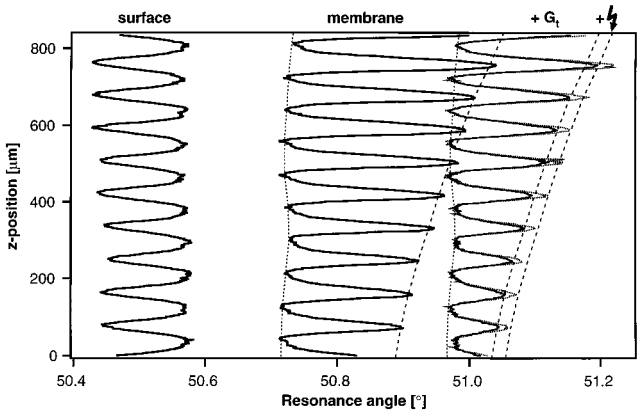

FIGURE 7: Spatial gradient of rhodopsin mass in a supported membrane. Overlayed scans (resonance angle vs *z*-position) at different steps in an experiment following the sequence: formation of a rhodopsin membrane → transducin binding → flash. The solvent-washed surface ("surface") shows a regular, homogeneous pattern of thiolipid lines (resonance at 50.57°) and CTA lines (resonance 50.44°). A rhodopsin membrane was assembled on this surface by mixed micelle dilution, preceded by a wash step with pure egg-PC/OG micelles. Stirring the cuvette slowly during this step led to a vertical gradient of rhodopsin-containing micelles in the cuvette, leading to a gradient in the mass of the finally established membrane ("membrane") on the CTA lines, but not on the thiolipid lines (compare dashed envelopes around the peaks of the structure). On CTA, the associated angle shifts range from 0.45° at *z*-position 80 μm to 0.60° at *z*-position 770 μm. On thiolipid lines, the variation in angle shifts is much smaller, ranging from 0.15° at $z = 40$ μm to 0.17° at $z = 40$ μm. Subsequent dark binding of transducin ("+G_t") shows no dependence on membrane mass, but only on surface type (mean angle shifts are 0.16° ± 0.008° on CTA, 0.25° ± 0.005° on thiolipid). A flash ("flash") leads to binding signals mainly on CTA regions (0.025° ± 0.004° on CTA, 0.004° ± 0.002° on thiolipid), which again are independent of membrane mass. The dashed envelopes are horizontally shifted with respect to each other, but not changed in shape.

Figure 6, trace b), so the incorporated rhodopsin seemed to be nonfunctional with respect to nucleotide exchange catalysis. Consequently, the binding signals on thiolipid surfaces must be interpreted with care: not all R* may be participating in the catalysis of transducin dissociation and desorption. Irreversible transducin binding was always low on thiolipid regions.

Transducin binding and desorption data from different experiments on pure and structured surfaces are summarized in Table 1. Lines 1 and 2 refer to the experiments shown also in Figure 6 (traces a and c); all other entries were obtained from structured samples. The following conclusions can be drawn from these and other experiments: (1) The mass of the prepared membranes was very variable. However, on thiolipid there was always less adsorbed material than on CTA. In spite of this variation, transducin binding to the membranes varied by only 20% (compare lines 2 and 4−6). (2) The relative transducin desorption amplitudes on CTA were always bigger than those on thiolipid, where no desorption at all was sometimes observed. (3) Transducin was released faster (in most cases much faster) from CTA than from thiolipid regions. (4) Release kinetics (in the presence of GTP) and the amplitudes of binding signals (in the absence of GTP) indicated similar densities of functional, correctly oriented rhodopsin in membranes on CTA, independent of the mass of the membrane. (5) Release rates on CTA regions depended almost linearly on the concentration of GTP (0.24 s^{-1} at 1 μM, 1.4 s^{-1} at 5 μM, 2.4 s^{-1} at 10 μM, lines 3, 4, 6). At GTP concentrations in the millimolar range, transducin release occurred much faster. On thiolipid, there was a trend to a slight increase of desorption rate with GTP concentration, but far less pronounced, suggesting rate limitation by another step, presumably R*−G_t interaction. (6) During flash-induced transducin desorption, pattern boundaries stayed as sharp as before, and desorption proceeded in parallel at all locations of the surface belonging to the same surface type (either thiolipid or CTA). No lateral gradients of transducin at the membrane were observed. There was no effect of different surface patterns on desorption rates.

In summary, the rhodopsin/transducin system in supported membranes reproduces characteristic features of its natural counterpart: (i) membrane binding of transducin with a binding constant in the micromolar range; (ii) light- and GTP-dependent transducin release by rhodopsin; (iii) linear dependence of rhodopsin activity on GTP concentration in the micromolar range; (iv) reversibility of transducin release. Finally, it is important to note that the type of surface employed clearly controls the rhodopsin activity: on thiolipid the activity was always lower than on CTA.

DISCUSSION

Rhodopsin has been reconstituted into planar phospholipid membranes, self-assembled onto functionalized gold surfaces, and served as a model for the investigation of G protein-coupled receptors with surface-sensitive optical techniques. Rhodopsin activity was assessed by its coupling to the G protein, transducin, following photoexcitation. Patterning of the supporting surface yielded membranes with spatially varying properties, resulting in a pattern of rhodopsin activity on the surface. All reaction steps, from membrane formation to transducin binding and release, were monitored in situ by one-dimensional imaging surface plasmon resonance. This technique is more precise than SPR microscopy (*48*), which has been used before to investigate biological recognition reactions on patterned surfaces (*49*, *50*, *70*). To our knowledge, this is the first application of 1D-SPR to biological membrane receptor systems.

CTA/Thiolipid Surfaces Are Well-Suited Supports for Self-Assembly of Phospholipid Bilayer and Monolayer Structures. Phospholipids are known to form either monolayers on densely-packed alkylthiol surfaces (*71*, *72*) and thiolipid surfaces (*32*) or bilayers on hydroxy- and carboxy-terminated thiol surfaces (*49*, *73*, *74*), analogously to oxide surfaces (*39*, *40*, *75*). For supported phospholipid bilayers, reported thickness values range from 42 Å [(*49*) POPC on hydroxy-thiols], to 43 Å [(*40*) DMPC on quartz], to 48 Å [(*74*) egg-PC on diethyleneglycol-functionalized gold surface]. For fully hydrated multilayers of DOPC, Wiener and White (*76*) measured a bilayer thickness of 44 Å. A supported POPC monolayer on a pure thiolipid surface was reported with 24 Å thickness (*32*). In this study, self-assembly of egg-PC on patterned CTA/thiolipid surfaces yielded stable membranes with a thickness of 47 Å on CTA and 26 Å on thiolipid. Given the cited literature values, we conclude from our results that a bilayer is routinely formed on CTA regions and a monolayer on thiolipid regions. Further support comes

from the observations that membranes resisted washing with 1 M salt, urea, or low detergent concentrations and that the membrane formation kinetics obtained from different spots on the surface agree perfectly. Thus, formation of pure egg-PC membranes by micelle dilution on CTA/thiolipid surfaces is quite a robust process, leading to very reproducibly stable and regular lipid mono- and bilayers.

The Density of Rhodopsin in Supported Membranes Is Comparable to Disk Membranes on CTA, but Distinctly Lower on Thiolipid. The procedure for rhodopsin reconstitution in supported membranes in this work was designed to fulfill the following criteria: (i) to avoid loss of rhodopsin functionality by always keeping the protein in contact either with detergent or with lipids; this is a profound difference to the method of Salamon et al. (*36*); (ii) relying on a defined system composed of a few, pure compounds, so that SPR data can be readily interpreted; (iii) exploiting the self-organizing properties of lipids to direct rhodopsin activity to certain surface areas. The latter point is unique in this work; published techniques for binding proteins or DNA to defined locations on a photopatterned surface relied, e.g., on coupling of photobiotin and streptavidin (*50*, *77*, *78*) or the use of photolabile silanes (*79*).

Rhodopsin membranes are thicker than pure lipid membranes on both surface types. Interestingly, the SPR spectra hardly broaden on membrane adsorption, which indicates, according to Rothenhäusler et al. (*80*), a very regular structure of the membranes. The rhodopsin densities on CTA calculated from this increase in membrane mass—rhodopsin per 20−30 nm^2—are comparable to the rhodopsin density in native disk membranes [1 rhodopsin/33 nm^2 (*81*)]. They are similar to those obtained by Salamon et al. (*36*) for rhodopsin in solvent-containing egg-PC membranes on silver, although their membranes are by far thicker.[3] In our system, the measured thickness of the membranes and the sharp minima in all SPR spectra indicate ordered bilayer structures. On thiolipid, the rhodopsin density is a factor of 2.5−6 lower than on CTA, depending on the assumptions made for the membrane structure.

Membrane Formation and Transducin Binding Data Indicate an Increase in the Effective Membrane Area upon Incorporation of Rhodopsin. If the excess mass of rhodopsin membranes compared to lipid membranes is not solely attributed to rhodopsin itself, an increase of 15−25% in effective membrane area must be assumed. This is in agreement with transducin binding data (see below). Explanations of this phenomenon would be either the presence of singly adsorbed vesicles on the planar membranes, attached via protein−protein contacts, since this does not occur in protein-free membranes, or the presence of a membrane with ripples on the molecular scale to accommodate extramembranous portions of rhodopsin between membrane and support, or both. The latter explanation is favored by the fact that rhodopsin membranes are very stable against washing with concentrated salt or urea and diluted detergent solutions.

[3] Salamon et al. measured 87 Å with a refractive index of $n = 1.62$, which would correspond to 213 Å at $n = 1.45$, as opposed to 67 Å in this work. A refractive index of around 1.62 has been measured only for a few highly halogenated organic compounds, and it is therefore very unlikely that such a value can be attributed to lipid membranes.

Transducin Binds Cooperatively and Similarly on Phospholipid Monolayer and Bilayer Regions. Transducin affinity is the same for pure lipid membranes on both surface types and for rhodopsin membranes on thiolipid. This indicates a similar lipid packing in these three cases (*82*). The G protein does not distinguish between a pure phospholipid bilayer and a bilayer composed of an outer phospholipid leaflet on a gold-attached thiolipid monolayer. The concentration at half-maximal binding (0.6−0.7 μM) is in the same range as that measured for pure disk membranes [0.3 μM (*17*)]. The same affinity is observed when rhodopsin is present in membranes on thiolipid, but the cooperativity of binding appears to be somewhat lower. Although the rhodopsin membrane on CTA contains 3−6 times more rhodopsin than that on thiolipid, this does not seem to change the overall binding capacity of the membrane for transducin, although it reduces its affinity 2.5-fold.

Positive cooperativity has been observed for binding of transducin to light-adapted ROS membranes (*83*); our experiments show that this cooperativity occurs to an even higher degree in pure lipid membranes and also in dark-adapted rhodopsin membranes. This cooperativity may be caused either by direct mutual interactions of transducin molecules or by a change in the properties of the lipid membrane on transducin binding, or by both of these effects. We did not pursue transducin titrations on light-adapted membranes because of the observed MII degradation with time.

Rhodopsin−Transducin Interaction on Supported Membranes Exhibits the Same Basic Reactions As Observed on Disk Membranes. As in light-scattering measurements on rod outer segments and disk membranes (*16*, *17*, *84*), we observed binding signals upon illuminating rhodopsin membranes in the absence of GTP. The density of R* (defined as active rhodopsin in the correct orientation to interact with G_t) in the membranes was determined from the amplitudes of these binding signals. On CTA, the density of R* was 1 per 600 nm^2; this value did not depend on membrane mass. In our experiments, addition of GTP led to dissociation signals, which have been also observed in light scattering experiments on disk membranes (*16*, *17*). This dissociation was reversible; eventually rebinding occurred, an effect also observed for disk membranes reconstituted with transducin (*84*). In rod cells, R* is deactivated within seconds by phosphorylation and arrestin binding (*3*, *7*), whereas in the reconstituted system (as in our case) bleached rhodopsin remains active for minutes. It slowly decays to MIII and opsin, a process with a half-time of 15 min (*5*, *86*); faster transducin rebinding is due to GTP being used up (*84*).

Continuous R* activity after a light flash, transducin rebinding as a function of GTP depletion, and slow R* decay have been demonstrated on supported membranes in this work. The application of GTP pulses of low concentration led to transducin desorption−rebinding cycles, the amplitude of which decreased with time. By demonstrating these three basic reactions of the rhodopsin/transducin system—binding, dissociation, rebinding—the current study goes beyond published SPR work (*36*).

The Kinetics of Transducin Release from Supported Bilayers Resemble Those Observed in Retinal Rods. An advantage of our measuring technique is that dissociation kinetics can be followed precisely without compromising

spatial resolution. In this section, we discuss the kinetics of transducin release on CTA surfaces. Homogeneous distribution of rhodopsin in the supported membranes is assumed and cooperative binding of transducin neglected for the moment. For transducin release to occur, the system must traverse a sequence of steps, formulated in the classical reaction scheme (*20*), which neglects substate multiplicity (*7*). The steps following flash and fast photoprocesses are as follows: (1) transition of rhodopsin from the MI to the active MII state (here termed R*, when correctly oriented in the supported membrane), which expresses the signalling state for G_t; (2) Diffusion of transducin toward MII; (3) binding of transducin to MII and GDP release; (4) GTP binding, dissociation of the subunits, release from MII; (5) release of the transducin subunits from the membrane.

Our observation is that the rate constant of the release kinetics (around 0.24 μM^{-1} s^{-1}) is proportional to GTP concentration in the range 1−10 μM. This strongly indicates that nucleotide exchange catalysis and subsequent dissociation of transducin into its subunits (step 4) are rate-limiting in this case. Transducin diffusion (step 2) is indeed expected to be much faster (>10 000 s^{-1}) at the equilibrium transducin density on the supported membrane, according to data from refs (*22* and *87*). Also the release of dissociated subunits from egg-PC bilayers (step 5) is considerably faster than the measured overall release rates in this study (*19*). Steps 1 and 3 are more critical (see below). Immediately after the flash, the transducin density on the membrane is still close to equilibrium. Under these conditions, and if all the other reactions are fast, the change in average transducin density on the membrane (SPR signal) is determined by

$$\frac{\partial \Theta}{\partial t} = -k_{cat}[\mathrm{GTP}]\frac{1}{N}$$

with Θ being the fraction of occupied transducin binding sites, [GTP] the GTP concentration, and N the number of transducin binding sites on the membrane per R*. k_{cat} is the catalytic rate constant of R* (step 4). In equilibrium, N = 10.8 transducin binding sites per activated rhodopsin (1 R* per 600 nm^2 and 1 transducin site per 56 nm^2). The experimentally determined overall release rate of 0.24 μM^{-1} s^{-1} then yields an intrinsic rate constant k_{cat} of 2.6 μM^{-1} s^{-1}. Literature values for the dissociation rate of the R^*G_t complex (in most cases extrapolated from low temperatures to room temperature) are in the same range: 10−15 μM^{-1} s^{-1} (*88*), 12 μM^{-1} s^{-1} (*20*), and 2000−8000 s^{-1} (*22*) at saturating concentrations of GTP [0.5−1 mM (*20, 69*)]. However, k_{cat} is probably a lower limit, since the MI−MII equilibrium is likely to be on the MI side under our conditions (*15*).

In membranes on CTA, the binding signals allow us to estimate that only 3−10% of the incorporated rhodopsin can be activated by a light flash. Denaturation of rhodopsin by contact with the CTA surface is unlikely, because (i) pure hydroxyl surfaces, which are similar apart from the charge, effectively resist protein adsorption (*89*) and (ii) the rhodopsin activity was very similar on negatively charged CTA and on positively charged aminothiol surfaces.[4] An explanation for the low fraction of active rhodopsin might be that its orientation in the membrane is not random. Again, since rhodopsin membranes on negatively and positively charged surfaces[4] showed similar activity, the oriented immobilization of rhodopsin due to electrostatic effects can be ruled out. Another reason might be glycosylation of rhodopsin at the extracytoplasmic side (*81*), which imposes steric constraints and might favor an orientation of rhodopsin with its cytoplasmic (transducin-binding) face toward the support, and thus inaccessible to the transducin.

Patterned Surfaces Induce a Pattern of Rhodopsin Activity in the Supported Membranes. Illumination of patterned supported rhodopsin membranes in the presence of GTP resulted in dissociation signals across the whole surface. But the kinetics were different between CTA and thiolipid regions: transducin dissociation was up to 12 times faster on CTA than on thiolipid. The observed residual transducin dissociation on thiolipid regions of structured surfaces may be due either to rhodopsin activity in these regions of the membrane or to lateral diffusion of transducin toward CTA regions where active rhodopsin molecules rapidly deplete the membrane of bound transducin, or both. Experiments on pure thiolipid surfaces suggest that active rhodopsin also may be present on thiolipid regions of structured surfaces, although to a variable degree (see Figure 6). Nevertheless, low reaction rates and the very weak GTP-dependence indicate that the coupling of R* to G_t (step 3 in the reaction scheme, see last section) becomes limiting for the overall rate of activation. This opens the possibility that lateral diffusion of transducin is responsible for the observed dissociation process from thiolipid regions. Bruckert et al. (*87*) used light scattering measurements on permeabilized ROS, where rhodopsin was activated by a pattern of interference fringes, to get information on the diffusion of transducin. With this complex system and with intrinsically small diffusion distances, it was only possible to give a lower limit of 0.8 μm^2 s^{-1} for the diffusion constant of transducin in the disk membrane. With this diffusion constant, transducin gradients should be observable on the supported membranes within seconds. However, no such gradients have been observed in our case. This does not exclude diffusion from one membrane region to another, but implies that the transition zone between membrane regions functions as a barrier. Present work in our laboratory concentrates on eliminating all possible rhodopsin activity from thiolipid regions; under such conditions of ideal contrast, the occurrence of dissociation signals in thiolipid regions would be a measure of transducin lateral diffusion.

CONCLUSION

Rhodopsin has been successfully reconstituted into planar patterned phospholipid membranes self-assembled onto gold surfaces. Coupling reactions with transducin were found to closely resemble those of the native system, indicating that the native functionality of rhodopsin was restored in the supported membranes. An influence of rhodopsin on the dark binding of transducin to lipid membranes could be demonstrated. Patterning of the supporting surface yielded membranes with spatially varying properties, resulting in a

[4] Positively charged hydrophilic surfaces were produced in the same way as CTA surfaces, but using mercaptoalkylamines. Membrane assembly, transducin binding, and release kinetics were found to closely resemble those of CTA surfaces.

pattern of rhodopsin activity on the surface. The advantage of our combination of molecularly structured surfaces with one-dimensional imaging SPR is that spatially varying processes at supported membranes can be resolved, e.g., lateral diffusion gradients of membrane-associated proteins. Addressable zones of receptor activity and density gradients, e.g., of antigenic peptides, can be created and binding and release reactions on different spots at the surface monitored in parallel and in real time. Future work will pursue the effort to enhance the contrast in receptor activity between different surface regions, and to extend the technique to include other components of the signal cascade.

ACKNOWLEDGMENT

We thank the following colleagues for their help: Kirsten Leufgen for performing TOF-SIMS experiments, and Claus Duschl, Martha Liley, Harald Seitz, and Martin Heck for helpful discussions and critical reading of the manuscript.

REFERENCES

1. Gilman, A. G. (1995) *Angew. Chem., Int. Ed. Engl. 34*, 1406−1419.
2. Hodgson, J. (1992) *Bio/Technology 9*, 973−980.
3. Helmreich, E. J. M., and Hofmann, K. P. (1996) *Biochim. Biophys. Acta 1996*, 285−322.
4. Gudermann, T., Kalkbrenner, F., and Schultz, G. (1996) *Annu. Rev. Pharmacol. Toxicol. 36*, 429−459.
5. Hofmann, K. P. (1986) *Photobiochem. Photobiophys. 13*, 309−327.
6. Hurley, J. B. (1992) *J. Bioenerg. Biomembr. 24*, 219−226.
7. Hofmann, K. P., Jäger, S., and Ernst, O. P. (1995) *Isr. J. Chem. 35*, 339−355.
8. Hargrave, P. A., Ed. (1993) *Photoreceptor cells* in *Methods in Neuroscience*, Academic Press, San Diego, CA.
9. Unger, V. M., and Schertler, G. F. X. (1995) *Biophys. J. 68*, 1776−1786.
10. Cone, R. A. (1972) *Nature (London), New Biol. 236*, 39−43.
11. Liebman, P. A., and Entine, G. (1974) *Science 185*, 457−459.
12. Khan, S. M., Bolen, W., Hargrave, P. A., Santoro, M. M., and McDowell, J. H. (1991) *Eur. J. Biochem. 200*, 53−59.
13. Mitchell, D. C., Straume, M., Miller, J. L., and Litman, B. J. (1990) *Biochemistry 29*, 9143−9149.
14. Ryba, N. J. P., and Marsh, D. (1992) *Biochemistry 31*, 7511−7518.
15. Gibson, N. J., and Brown, M. F. (1993) *Biochemistry 32*, 2438−2454.
16. Kühn, H., Bennett, N., Michel-Villaz, M., and Chabre, M. (1981) *Proc. Natl. Acad. Sci. U.S.A. 78* (*11*), 6873−6877.
17. Schleicher, A., and Hofmann, K. P. (1987) *J. Membr. Biol. 95*, 271−281.
18. Heck, M., and Hofmann, K. P. (1993) *Biochemistry 32*, 8220−8227.
19. Ernst, O. P., Hofmann, K. P., and Sakmar, T. P. (1995) *J. Biol. Chem. 270* (*18*), 10580−10586.
20. Kahlert, M., and Hofmann, K. P. (1991) *Biophys. J. 59*, 375−386.
21. Lamb, T. D., and Pugh, E. N. (1992) *J. Physiol. 449*, 719−758.
22. Felber, S., Breuer, H. P., Petruccione, F., Honerkamp, J., and Hofmann, K. P. (1996) *Biophys. J. 71*, 3051−3063.
23. Siebert, F. (1995) *Methods Enzymol. 246*, 501−526.
24. Arnis, S., and Hofmann, K. P. (1993) *Proc. Natl. Acad. Sci. U.S.A. 90* (*16*), 7849−7853.
25. McConnell, H. M., Owicki, J. C., Parce, J. W., Miller, D. L., Baxter, G. T., Wada, H. G., and Pitchford, S. (1992) *Science 257*, 1906−1912.
26. Lefkowitz, R. J., Cerione, R. A., Codina, J., Birnbaumer, L., and Caron, M. G. (1985) *J. Membr. Biol. 87*, 1−12.
27. Feder, D., Im, M.-J., Klein, H. W., Hekman, M., Holzhöfer, A., Dees, C., Levitzki, A., Helmreich, E. J. M., and Pfeuffer, T. (1986) *EMBO J. 5* (*7*), 1509−1514.
28. Knoll, W. (1991) *MRS Bull. 16* (*7*), 29−39.
29. Garland, P. B. (1996) *Q. Rev. Biophys. 29* (*1*), 91−117.
30. Hofmann, K. P. (1993) in *GTPases in Biology II* (Dickey, B., and Birnbaumer, L., Eds.) pp 267−290, Springer, Berlin.
31. Bain, C. D., Troughton, E. B., Tao, Y.-T., Evall, J., Whitesides, G. M., and Nuzzo, R. G. (1989) *J. Am. Chem. Soc. 111*, 321−335.
32. Lang, H., Duschl, C., and Vogel, H. (1994) *Langmuir 10*, 197−210.
33. Johnsson, B., Löfas, S., and Lindquist, G. (1991) *Anal. Chem. 198*, 268−277.
34. Malmqvist, M. (1993) *Curr. Opin. Immunol. 5*, 282−286.
35. Salafsky, J., Groves, J. T., and Boxer, S. G. (1996) *Biochemistry 35*, 14773−14781.
36. Salamon, Z., Wang, Y., Soulages, J. L., Brown, M. F., and Tollin, G. (1996) *Biophys. J. 71*, 283−294.
37. Tamm, L. K., and McConnell, H. M. (1985) *Biophys. J. 47*, 105−113.
38. McConnell, H. M., Watts, T. H., Weis, R. M., and Brian, A. A. (1986) *Biochim. Biophys. Acta 864*, 95−106.
39. Nollert, P., Kiefer, H., and Jähnig, F. (1995) *Biophys. J. 69*, 1447−1455.
40. Johnson, S. J., Bayerl, T. M., McDermott, D. C., Adam, G. W., Rennie, A. R., Thomas, R. K., and Sackmann, E. (1991) *Biophys. J. 59*, 289−294.
41. Heyse, S., Vogel, H., Sänger, M., and Sigrist, H. (1995) *Protein Sci. 4*, 2532−2544.
42. Liebman, P. A., Parker, K. R., and Dratz, E. A. (1987) *Annu. Rev. Physiol. 49*, 765−791.
43. Groves, J. T., Ulman, N., and Boxer, S. G. (1997) *Science 275*, 651−653.
44. Kumar, A., Abbott, N. L., Kim, E., Biebuyck, H. A., and Whitesides, G. M. (1995) *Acc. Chem. Res. 28*, 219−226.
45. Tarlov, M. J., Burgess, D. R. F., and Gillen, G. (1993) *J. Am. Chem. Soc. 115*, 5305−5306.
46. Duschl, C., Liley, M., and Vogel, H. (1994) *Angew. Chem., Int. Ed. Engl. 33* (*12*), 1274−1276.
47. Wollman, E. W., Frisbie, C. D., and Wrighton, M. S. (1993) *Langmuir 9*, 1517−1520.
48. Rothenhäusler, B., and Knoll, W. (1988) *Nature 332* (*6165*), 615−617.
49. Duschl, C., Liley, M., Corradin, G., and Vogel, H. (1994) *Biophys. J. 67*, 1229−1237.
50. Piscevic, D., Knoll, W., and Tarlov, M. J. (1995) *Supramol. Sci. 2*, 99−106.
51. Hickel, W., and Knoll, W. (1991) *Thin Solid Films 199*, 367−373.
52. Bain, C. D., and Whitesides, G. M. (1989) *Langmuir 5*, 1370−1378.
53. Fodor, S. P. A., Read, J. L., Pirrung, M. C., Stryer, L., Lu, A. T., and Solas, D. (1991) *Science 251*, 767−773.
54. Xiao, X., Zhao, C., Potash, H., and Nova, M. P. (1997) *Angew. Chem., Int. Ed. Engl. 36* (*7*), 780−782.
55. Kofod, H. (1963) *Org. Synth. Coll. Vol. IV*, 491.
56. Cook, R. M., Adams, J. H., and Hudson, D. (1994) *Tetrahedron Lett. 35*, 6777−6780.
57. Conrad, R. A., Cullinan, G. J., Gerzon, K., and Poore, G. A. (1979) *J. Med. Chem. 22*, 391−400.
58. de Grip, W. J. (1982) *Methods Enzymol. 81*, 197−207.
59. Huang, J., and Hemminger, J. C. (1993) *J. Am. Chem. Soc. 115*, 3342−3343.
60. Adamson, A. W. (1982) *Physical chemistry of surfaces*, p 664, Wiley & Sons, New York.
61. Rothenhäusler, B., and Knoll, W. (1987) *Surf. Sci. 191*, 585−594.
62. Spinke, J., Liley, M., Schmitt, F.-J., Guder, H.-J., Angermaier, L., and Knoll, W. (1993) *J. Chem. Phys. 99* (*9*), 7012−7019.
63. Reiter, R., Motschmann, H., and Knoll, W. (1993) *Langmuir 9* (*9*), 2430−2435.

64. Cuypers, P. A., Hermens, W. T., and Hemker, H. C. (1978) *Anal. Biochem. 84*, 56−67.
65. Arnebrandt, T., Ivarsson, B., Larsson, K., Lundström, I., and Nylander, T. (1985) *Prog. Colloid Polym. Sci. 70*, 62−66.
66. Spinke, J., Liley, M., Guder, H.-J., Angermaier, L., and Knoll, W. (1993) *Langmuir 9*, 1821−1825.
67. Stubbs, G. W., and Litman, B. J. (1978) *Biochemistry 17* (*2*), 215−219.
68. Lambright, D. G., Sondek, J., Bohm, A., Skiba, N. P., Hamm, H. E., and Sigler, P. B. (1996) *Nature 379*, 311−319.
69. Vuong, T. M., Chabre, M., and Stryer, L. (1984) *Nature 311*, 659−661.
70. Fischer, B., Heyn, S. P., Egger, M., and Gaub, H. E. (1993) *Langmuir 9*, 136−140.
71. Terrettaz, S., Stora, T., Duschl, C., and Vogel, H. (1993) *Langmuir 9*, 1361−1369.
72. Plant, A. L. (1993) *Langmuir 9*, 2764−2767.
73. Stelzle, M., Weissmüller, G., and Sackmann, E. (1993) *J. Phys. Chem. 97*, 2974−2981.
74. Williams, L. M., Evans, S. D., Flynn, T. M., Marsh, A., Knowles, P. F., Bushby, R. J., and Boden, N. (1997) *Langmuir 13*, 751−757.
75. Kalb, E., Frey, S., and Tamm, L. K. (1992) *Biochim. Biophys. Acta 1103*, 307−316.
76. Wiener, M. C., and White, S. H. (1992) *Biophys. J. 61*, 434−447.
77. Pritchard, D. J., Morgan, H., and Cooper, J. M. (1995) *Angew. Chem., Int. Ed. Engl. 34* (*1*), 91−93.
78. Sundberg, S. A., Barrett, R. W., Pirrung, M., Lu, A. L., Kiangsoontra, B., and Holmes, C. P. (1995) *J. Am. Chem. Soc. 117*, 12050−12057.
79. Chrisey, L. A., O'Ferrall, C. E., Spargo, B. J., Dulcey, C. S., and Calvert, J. M. (1996) *Nucleic Acids Res. 24* (*15*), 3040−3047.
80. Rothenhäusler, B., Rabe, J., Korpiun, P., and Knoll, W. (1984) *Surf. Sci. 137*, 373−383.
81. Hofmann, K. P., and Heck, M. (1996) *Biomembranes 2A*, 141−198.
82. Seitz, H. (1996) *Die Interaktion von Transducin und Lipidmembran*, Ph.D. Thesis, Fakultät für Physik, Universität Freiburg, Germany.
83. Williardson, B. M., Pou, B., Yoshida, T., and Bitensky, M. W. (1993) *J. Biol. Chem. 268* (*9*), 6371−6382.
84. Bennett, N., and Dupont, Y. (1985) *J. Biol. Chem. 260* (*7*), 4156−4168.
85. Kühn, H. (1980) *Nature 283*, 587−589.
86. Farrens, D. L., and Khorana, H. G. (1995) *J. Biol. Chem. 270* (*10*), 5073−5076.
87. Bruckert, F., Chabre, M., and Vuong, T. M. (1992) *Biophys. J. 63*, 616−629.
88. Kohl, B., and Hofmann, K. P. (1987) *Biophys. J. 52*, 271−277.
89. Prime, K. L., and Whitesides, G. M. (1993) *J. Am. Chem. Soc. 115*, 10714−10721.

BI971564R